PHYSICAL REVIEW B **103**, L020405 (2021)

Letter

Anomalous Hall resistivity and possible topological Hall effect in the EuAl$_4$ antiferromagnet

T. Shang,[1,2,*] Y. Xu,[3,†] D. J. Gawryluk,[2] J. Z. Ma,[4,5] T. Shiroka,[6,7] M. Shi,[5] and E. Pomjakushina[2,‡]
[1]*Key Laboratory of Polar Materials and Devices (MOE), School of Physics and Electronic Science, East China Normal University, Shanghai 200241, China*
[2]*Laboratory for Multiscale Materials Experiments, Paul Scherrer Institut, CH-5232 Villigen PSI, Switzerland*
[3]*Physik-Institut, Universität Zürich, Winterthurerstrasse 190, CH-8057 Zürich, Switzerland*
[4]*Department of Physics, City University of Hong Kong, Kowloon, Hong Kong*
[5]*Swiss Light Source, Paul Scherrer Institut, CH-5232 Villigen PSI, Switzerland*
[6]*Laboratorium für Festkörperphysik, ETH Zürich, CH-8093 Zurich, Switzerland*
[7]*Laboratory for Muon-Spin Spectroscopy, Paul Scherrer Institut, CH-5232 Villigen PSI, Switzerland*

(Received 21 October 2020; accepted 2 December 2020; published 11 January 2021)

We report the observation of anomalous Hall resistivity in single crystals of EuAl$_4$, a centrosymmetric tetragonal compound, which exhibits coexisting antiferromagnetic (AFM) and charge-density-wave (CDW) orders with onset at $T_N \sim 15.6$ K and $T_{CDW} \sim 140$ K, respectively. In the AFM state, when the magnetic field is applied along the *c*-axis direction, EuAl$_4$ undergoes a series of metamagnetic transitions. Within this field range, we observe a clear humplike anomaly in the Hall resistivity, representing part of the anomalous Hall resistivity. By considering different scenarios, we conclude that such a humplike feature is most likely a manifestation of the topological Hall effect, normally occurring in noncentrosymmetric materials known to host nontrivial topological spin textures. In view of this, EuAl$_4$ would represent a rare case where the topological Hall effect not only arises in a centrosymmetric structure, but it also coexists with CDW order.

DOI: 10.1103/PhysRevB.103.L020405

Introduction. The Hall effect, involving either the charge or the spin degree of freedom, is at the research frontier due to its possible applications in spintronic devices [1–3]. In the charge channel, the Hall resistivity ρ_{xy} in a magnetic material can generally be decomposed into two components, $\rho_{xy} = \rho_{xy}^O + \rho_{xy}^A$, where ρ_{xy}^O and ρ_{xy}^A represent the ordinary and the anomalous Hall resistivity, respectively. Further on, ρ_{xy}^A can be split into a conventional anomalous Hall term $\rho_{xy}^{A'}$, mostly determined by the magnetization M and the electrical resistivity ρ_{xx}, and a topological Hall term ρ_{xy}^T. The topological Hall effect is considered the hallmark of spin textures with a finite scalar spin chirality in real space [4–15]. Such topological spin textures exhibit a nonzero Berry phase, which acts as an effective magnetic field and gives rise to topological Hall resistivity, namely, ρ_{xy}^T. Among the notable examples in this regard are the noncentrosymmetric MnSi and analog compounds [4–7], where ρ_{xy}^T is caused by magnetic skyrmions.

The tetragonal BaAl$_4$-type structure represents the prototype for many binary and ternary derivative compounds [16]. The research on tetragonal *AE*(Al,Ga)$_4$ (*AE* = Sr, Ba, and Eu) materials was recently reinvigorated by the discovery of nontrivial band topology in BaAl$_4$, where also a giant magnetoresistance (MR) was observed [17]. Both BaAl$_4$ and BaGa$_4$ exhibit metallic behavior without showing any phase transition, while SrAl$_4$ shows a charge-density-wave (CDW) and a structural phase transition at $T_{CDW} \sim 250$ K and $T_S \sim 90$ K, respectively [18]. Unlike its nonmagnetic counterparts, EuGa$_4$ is an antiferromagnet below $T_N \sim 16.5$ K, while EuAl$_4$ undergoes a series of antiferromagnetic (AFM) transitions in its CDW ordered state [19–24]. Clearly, in the Eu(Al,Ga)$_4$ family, the 4*f* electrons bring new intriguing aspects to the topology.

Most of the previous work on Eu(Al,Ga)$_4$ has focused on their temperature-dependent properties, with the electrical transport properties under applied magnetic fields being somewhat overlooked [19–24]. Here, we report the observation of a humplike anomaly in the Hall resistivity of EuAl$_4$ single crystal. Since such anomaly appears in the magnetic field region where a series of metamagnetic transitions take place, most likely it is caused by the topological spin textures. Yet, we consider also the possibility of a regular origin of such anomaly in the Hall resistivity.

Experimental details. Single crystals of EuAl$_4$ were grown by a molten Al flux method. The crystals were checked by powder x-ray diffraction (XRD) measured using a Bruker D8 diffractometer. No extraneous phases could be identified in the XRD pattern, while Rietveld refinement confirmed the tetragonal crystal structure ($I4/mmm$, No. 139) with lattice parameters $a = b = 4.400$ Å and $c = 11.167$ Å. Magnetization and electrical resistivity measurements were performed in a Quantum Design magnetic properties measurement system and physical property measurement system, respectively. For the resistivity measurements, the electric current was applied in the *ab* plane, while the magnetic field was applied along the *c* axis. To avoid spurious resistivity contributions due to misaligned Hall probes, all the resistivity measurements were performed in both positive and negative magnetic fields. Then,

---

[*] tian.shang@psi.ch
[†] yangxu@physik.uzh.ch
[‡] ekaterina.pomjakushina@psi.ch

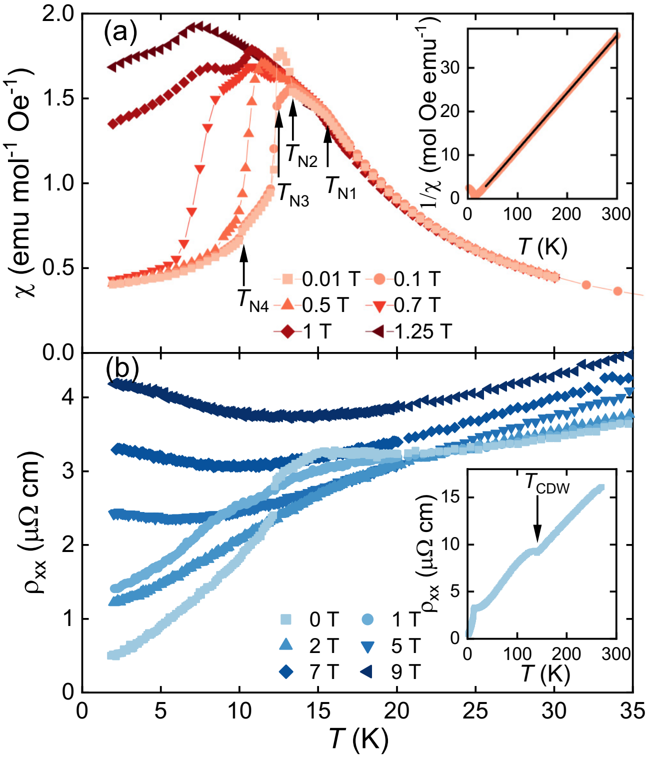

FIG. 1. Temperature dependence of (a) magnetic susceptibility $\chi(T,H)$ and (b) electrical resistivity $\rho_{xx}(T,H)$ of EuAl$_4$, measured in various applied magnetic fields. The arrows in (a) denote the four different magnetic transitions. The insets show the 0.1-T inverse susceptibility $\chi(T)^{-1}$ (top) and the zero field $\rho_{xx}(T)$ up to $\sim$300 K (bottom). The solid line in the top inset is a fit to the Curie-Weiss law, whereas the arrow in the bottom inset marks the CDW transition occurring at $T_{\mathrm{CDW}} \sim 140$ K.

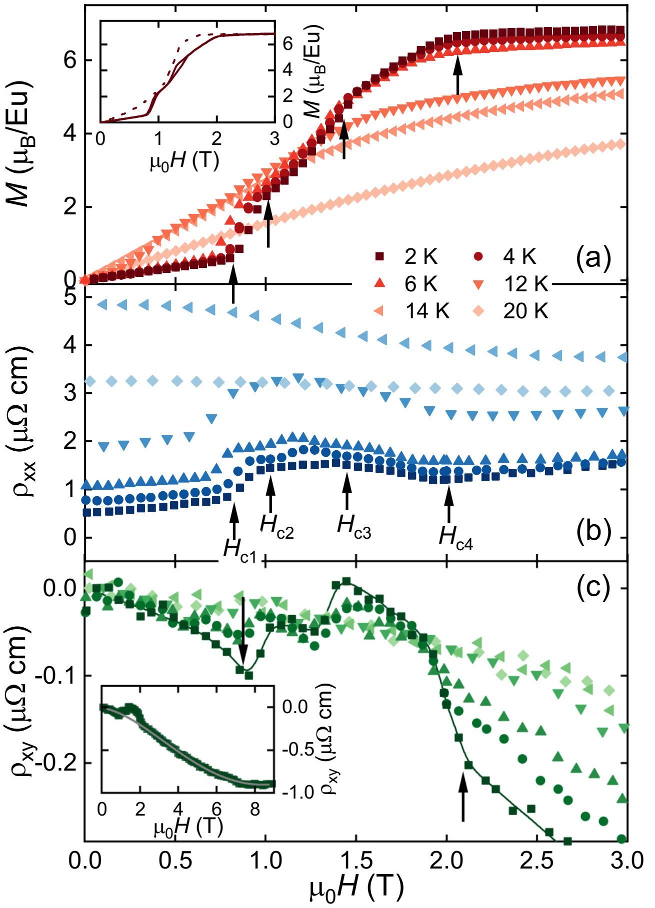

FIG. 2. Field dependence of (a) magnetization $M(H,T)$, (b) electrical resistivity $\rho_{xx}(H,T)$, and (c) Hall resistivity $\rho_{xy}(H,T)$ of EuAl$_4$, collected at various temperatures. The arrows in panels (a) and (b) mark the saturation field (H_{c4}) and the three critical fields (H_{c1}, H_{c2}, and H_{c3}) where EuAl$_4$ undergoes metamagnetic transitions. The arrows in (c) denote the upper and lower field limit, where the humplike anomaly appears in the $\rho_{xy}(H,T)$ data. The inset in (a) shows the 2-K magnetization, with the magnetic field applied along the c axis (solid line) or in the ab plane (dashed line). The inset in (c) shows the 2-K $\rho_{xy}(H)$ resistivity data up to 9 T, with the solid line being a polynomial fit.

in the case of the Hall resistivity ρ_{xy}, the spurious longitudinal contribution was removed by an antsymmetrization procedure, i.e., $\rho_{xy}(H) = [\rho_{xy}(H) - \rho_{xy}(-H)]/2$. Whereas in the case of the longitudinal electrical resistivity ρ_{xx}, the spurious transverse contribution was removed by a symmetrization procedure, i.e., $\rho_{xx}(H) = [\rho_{xx}(H) + \rho_{xx}(-H)]/2$.

Results and discussion. The temperature dependence of the magnetic susceptibility $\chi(T,H)$ and electrical resistivity $\rho_{xx}(T,H)$ of EuAl$_4$, measured under various magnetic fields, are shown in Fig. 1. Four successive antiferromagnetic transitions can be clearly identified in the $\chi(T)$ measured in a small magnetic field (<0.1 T), as indicated by the arrows in Fig. 1(a). The zero-field-cooling and field-cooling magnetic susceptibilities are practically identical, thus confirming the AFM nature of these transitions. The transition temperatures, $T_{\mathrm{N1}} \sim 15.6$, $T_{\mathrm{N2}} \sim 13.4$, $T_{\mathrm{N3}} \sim 12.6$, and $T_{\mathrm{N4}} \sim 10.2$ K, are in good agreement with those of previous studies [21,22]. The inset in Fig. 1(a) shows a Curie-Weiss fit to the inverse susceptibility (for $T > 20$ K), which yields an effective magnetic moment $\mu_{\mathrm{eff}} \sim 7.77\mu_{\mathrm{B}}$ and a paramagnetic Curie temperature $\theta_{\mathrm{p}} \sim 14.5$ K. The effective moment is close to the theoretical value for free Eu^{2+} ions ($7.94\mu_{\mathrm{B}}$). The AFM transitions can also be identified in the temperature-dependent $\rho_{xx}(T)$ data, yet they become less visible in an applied magnetic field. By contrast, the transitions are more evident in the field-dependent resistivity $\rho_{xx}(H)$ (see below). The high-T resistivity data are shown in the inset of Fig. 1(b). Here, the distinct anomaly at $T_{\mathrm{CDW}} \sim 140$ K is attributed to the gap opening near a CDW transition [19–24], yet more direct evidence is still missing. Another notable feature in Fig. 1(b) is the giant MR at base temperature, reaching $\sim$800% at 9 T. Since similar MR values have been reported also in nonmagnetic BaAl$_4$ [17], the magnetic nature of Eu^{2+} ions cannot account for the appearance of magnetoresistance in EuAl$_4$.

Figure 2 shows the field dependence of the magnetization $M(H,T)$, electrical resistivity $\rho_{xx}(H,T)$, and Hall resistivity $\rho_{xy}(H,T)$ of EuAl$_4$ at various temperatures, with the field applied along the c axis. The selected temperatures cover both the antiferromagnetic and the paramagnetic states. In the AFM state (below 16 K), EuAl$_4$ undergoes three metamagnetic transitions as the field increases. At each transition, $M(H)$ shows a small yet clear hysteresis [see inset in Fig. 2(a)]. By contrast, with the applied field in the *ab* plane, the metamagnetic transitions and the hysteresis are both less evident (see dashed line). At base temperature, the magnetization saturates when the external field is larger than $\mu_0 H_{c4} \sim 2.1$ T. For both field orientations, the saturation magnetization $M_s \sim 6.8\mu_B$ is consistent with $7.0\mu_B$, the expected value for the $J = 7/2$ Eu^{2+} ions. For $H < H_{c4}$, as indicated by arrows in Fig. 2(a), $\mathrm{EuAl_4}$ undergoes three metamagnetic transitions at $\mu_0 H_{c1} \sim 0.8$ T, $\mu_0 H_{c2} \sim 1.1$ T, and $\mu_0 H_{c3} \sim 1.5$ T, respectively. The metamagnetic transitions are tracked also in the $\rho_{xx}(H)$ data. All the critical fields, as determined from $\rho_{xx}(H, T)$, are highly consistent with the magnetization results (see phase diagram below).

In the AFM state, in the field range between H_{c1} (first metamagnetic transition) and H_{c4} (saturation of magnetization), $\rho_{xy}(H, T)$ exhibits a humplike anomaly [see Fig. 2(c)], reminiscent of the topological Hall resistivity arising from topological spin textures [4–15]. The anomaly, particularly evident at low temperatures, becomes almost invisible above 12 K. In general, to determine the topological contribution ρ^T_{xy}, the ordinary (ρ^O_{xy}) and the conventional anomalous ($\rho^{A'}_{xy}$) contributions have to be subtracted from the measured ρ_{xy}. In $\mathrm{EuAl_4}$, owing to its giant MR and the multiband origin of its ordinary Hall resistivity, such procedure is not feasible. The multiband nature of ρ_{xy} is clearly evident from its nonlinear behavior for $\mu_0 H > 6$ T [see inset in Fig. 2(c) and Ref. [20]]. This becomes even more robust upon applying a magnetic field in the *ab* plane, thus making the subtraction of ρ^O_{xy} unreliable. We recall that also the nonmagnetic $\mathrm{BaAl_4}$ shows a multiband Hall resistivity in a wide temperature range [17].

Since the humplike Hall resistivity appears only in a narrow field range, to extract the hump anomaly $\Delta\rho_{xy}(H)$ we may simply subtract a polynomial background [see black line in the inset of Fig. 2(c)]. Note that $\Delta\rho_{xy}$ is part of the anomalous Hall resistivity, i.e., it might be either trivial (conventional anomalous Hall resistivity $\rho^{A'}_{xy}$) or nontrivial (topological Hall resistivity ρ^T_{xy}). Independent of its nature, the derived $\Delta\rho_{xy}(H)$ at different temperatures are shown in Figs. 3(a) and 3(b) (the latter as a contour plot). Clearly, $\Delta\rho_{xy}$ is most prominent at temperatures below T_{N3} and in the field range between H_{c3} and H_{c4}, where the Eu^{2+} moments undergo a third metamagnetic transition and become fully polarized.

Now we discuss the different methods to decompose the measured Hall resistivity and hence track the origin of its humplike anomaly. To check whether a nonzero ρ^T_{xy} underlies the hump in $\rho_{xy}(H)$, a knowledge of the exact field evolution of the ordinary $\rho^O_{xy}(H)$ and conventional anomalous Hall contributions $\rho^{A'}_{xy}(H)$ is crucial. On the one hand, as a compensated metal [20,25], $\mathrm{EuAl_4}$ exhibits multiple bands crossing the Fermi level, as confirmed experimentally by de Haas–van Alphen and photoelectron spectroscopy, and theoretically by band structure calculations [21,22,24]. The ordinary Hall resistivity was previously analyzed using a two-carrier model in the paramagnetic state of $\mathrm{EuAl_4}$ [20]. While in the AFM state, such model becomes unreliable due to the presence of anomalous contributions. In this case, $\rho^O_{xy}(H)$ is unknown *a priori*, but it is presumably a nonlinear function of field. On the other hand, the conventional anomalous Hall resistivity $\rho^{A'}_{xy}$ is even more complex to extract from the data. Initially, $\rho^{A'}_{xy}(H)$ was evaluated as $R_s M(H)$, with R_s a constant and $M(H)$ the field-dependent magnetization [26]. Later on it was recognized that the coefficient R_s is not a constant, but rather a function of the field-dependent longitudinal electrical resistivity $\rho_{xx}(H)$ [27]. Consequently, $\rho^{A'}_{xy}$ can be rewritten as $S_H \rho^2_{xx} M$ or $S'_H \rho_{xx} M$. In real materials, $\rho^{A'}_{xy}$ depends on the mechanisms of intrinsic, side-jump, or skew scattering, or an intricate combination thereof [26,28,29]. These different representations, together with the multiband nature of $\mathrm{EuAl_4}$, make the extraction of ρ^T_{xy} from the measured ρ_{xy} even more complicated, especially considering the presence of a giant MR (implying a large ρ_{xx}) in $\mathrm{EuAl_4}$. Below we discuss in detail three possible scenarios.

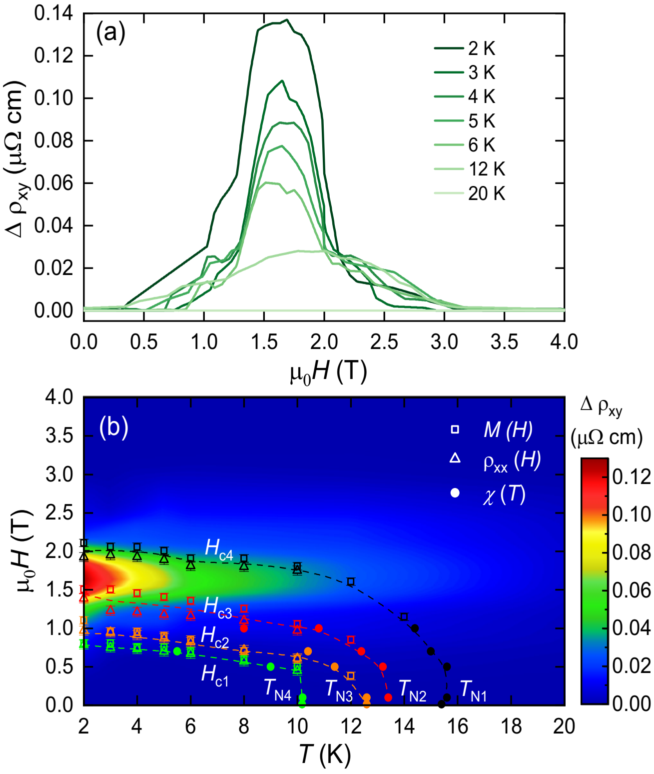

FIG. 3. (a) Field dependence of the extracted $\mathrm{EuAl_4}$ Hall resistivity $\Delta\rho_{xy}(H)$ at various temperatures (see text for the definition of $\Delta\rho_{xy}$). (b) Magnetic phase diagram of an $\mathrm{EuAl_4}$ single crystal, with the field applied along the *c* axis. The critical temperatures (T_{N1} to T_{N4}) are determined from $\chi(T, H)$ (circles), while the critical fields are determined from $M(H, T)$ (squares) and $\rho_{xx}(H, T)$ (triangles). The background color in (b) represents the magnitude of $\Delta\rho_{xy}(H)$ at various temperatures. The dashed lines are guides to the eyes. The error bars correspond to the field steps in the field-swept measurements.

Scenario I: $\rho^{A'}_{xy}$ proportional to M. Despite its simplicity, this scenario has often been used, especially in ferromagnets [26,30]. The $M(H)$ data in Fig. 4(a) show that the magnetization of $\mathrm{EuAl_4}$ undergoes steplike metamagnetic transitions, to finally saturate above 2.1 T. Consequently, in principle, $\rho^{A'}_{xy}$ should exhibit similar features to the magnetization. However, instead of a steplike feature, a humplike anomaly was observed in the Hall resistivity of $\mathrm{EuAl_4}$. Clearly, if this

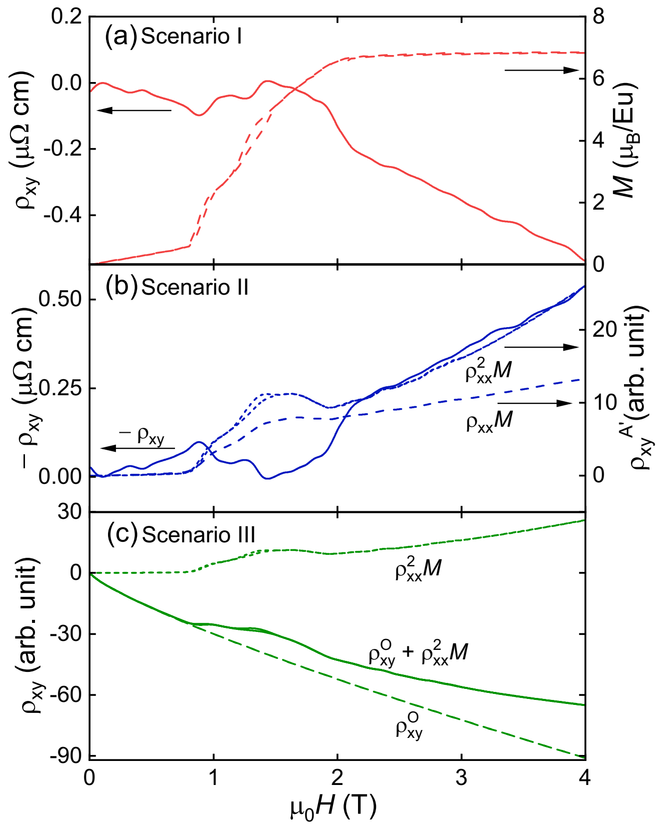

FIG. 4. Possible scenarios for extracting the topological contribution from the measured Hall resistivity of an $\mathrm{EuAl_4}$ single crystal. (a) Field-dependent Hall resistivity and magnetization. (b) Calculated $\rho_{xy}^{A'}(H)$. To compare it with the measured $\rho_{xy}(H)$, a scaling factor was used for calculating $\rho_{xy}^{A'}$ from ρ_{xx} and M. (c) Simulated field-dependent ρ_{xy}. The ordinary term is assumed to follow $\rho_{xy}^{O} \propto H^{0.8}$. All the results refer to the data at 2 K.

scenario applies, $\rho_{xy}^{A'}$ contributes negligibly to the total ρ_{xy}. This implies that the humplike anomaly is basically due to the topological ρ_{xy}^{T} term, most likely caused by topological spin textures.

Scenario II: $\rho_{xy}^{A'}$ proportional to $\rho_{xx}^2 M$ or $\rho_{xx} M$ with a negative prefactor. If the prefactors S_H and S_H' are allowed to be negative, then the hump anomaly in $\rho_{xx}^2 M(H)$ or $\rho_{xx} M(H)$ is convex [see Fig. 4(b)], which is opposite to the concave feature in $-\rho_{xy}(H)$. Since both $M(H)$ and $\rho_{xx}(H)$ are positive, a negative sign is necessary to overlap the calculated $\rho_{xy}^{A'}$ with the measured ρ_{xy}, which is negative at high magnetic fields [see $\rho_{xy}(H)$ in Fig. 4(a)]. In this case, a subtraction of $\rho_{xy}^{A'}$ from ρ_{xy} enhances the hump feature, i.e., it increases the magnitude of $\Delta\rho_{xy}$. Again, such scenario implies that the anomaly in ρ_{xy} must come from a topological term ρ_{xy}^{T}, and the extracted $\Delta\rho_{xy}$ shown in Fig. 3 represents a lower limit to the intrinsic value of ρ_{xy}^{T}. This scenario was successfully applied to extract the ρ_{xy}^{T} in EuPtSi, whose A phase is proposed to host magnetic skyrmions [31].

Scenario III: $\rho_{xy}^{A'}$ proportional to $\rho_{xx}^2 M$ or $\rho_{xx} M$ with a positive prefactor. If the prefactors S_H and S_H' are allowed to be positive, then the outcome could be different. We simulated the behavior of $\rho_{xy}(H)$ by combining ρ_{xy}^{O} and $\rho_{xx}^2 M$, assuming that $\rho_{xy}^{O}(H)$ follows an $H^{0.8}$ dependence. As shown by the solid line in Fig. 4(c), the simulated $\rho_{xy}(H)$ qualitatively agrees with the measured $\rho_{xy}(H)$. In this case, the hump anomaly in ρ_{xy} is trivial, being closely related to $\rho_{xy}^{A'}$, and no additional ρ_{xy}^{T} contribution needs to be invoked. However, even in such case, a finite ρ_{xy}^{T} might still exist, although mostly masked by $\rho_{xy}^{A'}$. This underlying topological component, though difficult to isolate, can still contribute to the hump anomaly in ρ_{xy}, as shown, e.g., in $\mathrm{EuCd_2As_2}$ and CeAlGe [32,33]. In this case, the extracted $\Delta\rho_{xy}$ shown in Fig. 3 represents an upper limit to the intrinsic value of ρ_{xy}^{T}.

Depending on which scenario applies, the interpretation of Hall resistivity data of $\mathrm{EuAl_4}$ is different. Now we further discuss the nontrivial origin of the humplike anomaly in ρ_{xy}. The observation of a topological Hall effect is usually attributed to noncoplanar spin textures, such as magnetic skyrmions, characterized by a finite scalar spin chirality in real space. These spin textures are often observed in magnetic materials that lack an inversion symmetry, and can be stabilized by the Dzyaloshinskii-Moriya interaction [34–40]. Conversely, magnetic materials with a centrosymmetric crystal structure that still host magnetic skyrmions are rare. To date, only a few systems have been reported, including $\mathrm{Gd_2PdSi_3}$ [11], $\mathrm{Gd_3Ru_4Al_{12}}$ [41], $\mathrm{Fe_3Sn_2}$ [42], and recently $\mathrm{GdRu_2Si_2}$ [43]. Compared to noncentrosymmetric systems, skyrmions in centrosymmetric materials exhibit the unique advantages of tunable skyrmion size and spin helicity [44]. In centrosymmetric systems, for example, skyrmions can be stabilized either by magnetic frustration (e.g., in $\mathrm{Gd_3Ru_4Al_{12}}$, $\mathrm{Gd_2PdSi_3}$, and $\mathrm{Fe_3Sn_2}$), or by the competition between the magnetic interactions and magnetic anisotropies (e.g., in $\mathrm{GdRu_2Si_2}$) [11,41–43,45]. In the $\mathrm{EuAl_4}$ case, as shown in the inset of Fig. 2(a), the magnetic anisotropy is moderate. Yet, according to recent NMR studies, $\mathrm{EuAl_4}$ exhibits a clear anisotropic Knight shift as the temperature approaches T_N [46]. Since $\mathrm{EuAl_4}$ adopts the same crystal structure of $\mathrm{GdRu_2Si_2}$, skyrmions might be stabilized by the same mechanism. More interestingly, if topological spin textures indeed exist in the AFM phase of $\mathrm{EuAl_4}$, this would represent a rare case where a rather exotic magnetic order coexists with CDW order.

Apart from the above topological spin textures, upon breaking certain symmetries, noncollinear antiferromagnets may also exhibit a topological Hall effect due to crossings or anticrossings of bands with a significant Berry curvature, as e.g., at the Weyl points [47]. Such a momentum-space scenario has been theoretically proposed and experimentally observed, for instance, in $\mathrm{Mn_3Sn}$ [48,49], GdPtBi [50], YbPtBi [51], and $\mathrm{Mn_3Ge}$ [52]. A three-dimensional Dirac spectrum with nontrivial topology and possible nodal lines crossing the Brillouin zone was recently observed in nonmagnetic $\mathrm{BaAl_4}$ [17]. In this context, a topologically nontrivial band structure is also expected in magnetic $\mathrm{EuAl_4}$, extending beyond its magnetically ordered state.

In summary, we observed a humplike anomaly $\Delta\rho_{xy}$ in the Hall resistivity of the centrosymmetric antiferromagnet $EuAl_4$ (single crystal). By systematic field- and temperature-dependent electrical resistivity and magnetization measurements, we could establish the magnetic phase diagram of $EuAl_4$. The $\Delta\rho_{xy}$ anomaly appears mostly in a field range where also metamagnetic transitions occur. Depending on the scenario used for evaluating the conventional anomalous Hall resistivity, the observed $\Delta\rho_{xy}$ corresponds to a topological Hall term ρ^T_{xy}, or to the lower/upper limits of the topological contribution. Although a trivial origin of the effect cannot be fully excluded, our results suggest that a topological Hall effect and topological spin textures may indeed exist in $EuAl_4$. To confirm such topological magnetic phase in $EuAl_4$, further experiments, such as resonant x-ray scattering or Lorentz transmission electron microscopy, are highly desirable. $EuAl_4$ represents a rare case where both geometrical frustration and inversion symmetry breaking are absent. Hence, it may offer a candidate compound for exploring the skyrmion physics and its applications in materials with a simple crystal structure.

Acknowledgments. We thank M. Medarde for the assistance during the electrical resistivity and magnetization measurements. T.S. acknowledges support from the Schweizerische Nationalfonds zur Förderung der Wissenschaftlichen Forschung (SNF) (Grants No. 200021_188706 and No. 206021_139082). Y.X. was supported by SNF via Grants No. 206021_139082 and No. PP00P2_179097. This work was partially supported also by the National Natural Science Foundation of China (Grants No. 11674336 and No. 11874150) and the Sino-Swiss Science and Technology Cooperation (Grant No. IZLCZ2-170075).

---

[1] N. Nagaosa and Y. Tokura, Topological properties and dynamics of magnetic skyrmions, Nat. Nanotechnol. **8**, 899 (2013).

[2] J. Sinova, S. O. Valenzuela, J. Wunderlich, C. H. Back, and T. Jungwirth, Spin Hall effects, Rev. Mod. Phys. **87**, 1213 (2015).

[3] A. Hirohata, K. Yamada, Y. Nakatani, I.-L. Prejbeanu, B. Diény, P. Pirro, and B. Hillebrands, Review on spintronics: Principles and device applications, J. Magn. Magn. Mater. **509**, 166711 (2020).

[4] A. Neubauer, C. Pfleiderer, B. Binz, A. Rosch, R. Ritz, P. G. Niklowitz, and P. Böni, Topological Hall Effect in the *A* Phase of MnSi, Phys. Rev. Lett. **102**, 186602 (2009).

[5] J. Gayles, F. Freimuth, T. Schena, G. Lani, P. Mavropoulos, R. A. Duine, S. Blügel, J. Sinova, and Y. Mokrousov, Dzyaloshinskii-Moriya Interaction and Hall Effects in the Skyrmion Phase of $Mn_{1-x}Fe_xGe$, Phys. Rev. Lett. **115**, 036602 (2015).

[6] N. Kanazawa, Y. Onose, T. Arima, D. Okuyama, K. Ohoyama, S. Wakimoto, K. Kakurai, S. Ishiwata, and Y. Tokura, Large Topological Hall Effect in a Short-Period Helimagnet MnGe, Phys. Rev. Lett. **106**, 156603 (2011).

[7] C. Franz, F. Freimuth, A. Bauer, R. Ritz, C. Schnarr, C. Duvinage, T. Adams, S. Blügel, A. Rosch, Y. Mokrousov, and C. Pfleiderer, Real-Space and Reciprocal-Space Berry Phases in the Hall Effect of $Mn_{1-x}Fe_xSi$, Phys. Rev. Lett. **112**, 186601 (2014).

[8] T. Schulz, R. Ritz, A. Bauer, M. Halder, M. Wagner, C. Franz, C. Pfleiderer, K. Everschor, M. Garst, and A. Rosch, Emergent electrodynamics of skyrmions in a chiral magnet, Nat. Phys. **8**, 301 (2012).

[9] Q. Qin, L. Liu, W. Lin, X. Shu, Q. Xie, Z. Lim, C. Li, S. He, G. M. Chow, and J. Chen, Emergence of topological Hall effect in a $SrRuO_3$ single layer, Adv. Mater. **31**, 1807008 (2019).

[10] J. Matsuno, N. Ogawa, K. Yasuda, F. Kagawa, W. Koshibae, N. Nagaosa, Y. Tokura, and M. Kawasaki, Interface-driven topological Hall effect in $SrRuO_3$-$SrIrO_3$ bilayer, Sci. Adv. **2**, e1600304 (2016).

[11] T. Kurumaji, T. Nakajima, M. Hirschberger, A. Kikkawa, Y. Yamasaki, H. Sagayama, H. Nakao, Y. Taguchi, T.-h. Arima, and Y. Tokura, Skyrmion lattice with a giant topological Hall effect in a frustrated triangular-lattice magnet, Science **365**, 914 (2019).

[12] N. Kanazawa, Y. Nii, X.-X. Zhang, A. S. Mishchenko, G. De Filippis, F. Kagawa, Y. Iwasa, N. Nagaosa, and Y. Tokura, Critical phenomena of emergent magnetic monopoles in a chiral magnet, Nat. Commun. **7**, 11622 (2016).

[13] Y. Fujishiro, N. Kanazawa, T. Nakajima, X. Z. Yu, K. Ohishi, Y. Kawamura, K. Kakurai, T. Arima, H. Mitamura, A. Miyake, K. Akiba, M. Tokunaga, A. Matsuo, K. Kindo, T. Koretsune, R. Arita, and Y. Tokura, Topological transitions among skyrmion- and hedgehog-lattice states in cubic chiral magnets, Nat. Commun. **10**, 1059 (2019).

[14] B. Göbel, C. A. Akosa, G. Tatara, and I. Mertig, Topological Hall signatures of magnetic hopfions, Phys. Rev. Res. **2**, 013315 (2020).

[15] L. Vistoli, W. Wang, A. Sander, Q. Zhu, B. Casals, R. Cichelero, A. Barthélémy, S. Fusil, G. Herranz, S. Valencia, R. Abrudan, E. Weschke, K. Nakazawa, H. Kohno, J. Santamaria, W. Wu, V. Garcia, and M. Bibes, Giant topological Hall effect in correlated oxide thin films, Nat. Phys. **15**, 67 (2019).

[16] F. Kneidinger, L. Salamakha, E. Bauer, I. Zeiringer, P. Rogl, C. Blaas-Schenner, D. Reith, and R. Podloucky, Superconductivity in noncentrosymmetric $BaAl_4$ derived structures, Phys. Rev. B **90**, 024504 (2014).

[17] K. Wang, R. Mori, Z. Wang, L. Wang, J. H. S. Ma, D. W. Latzke, D. E. Graf, J. D. Denlinger, D. Campbell, B. A. Bernevig, A. Lanzara, and J. Paglione, Crystalline symmetry-protected non-trivial topology in prototype compound $BaAl_4$, arXiv:2007.12571.

[18] A. Nakamura, T. Uejo, H. Harima, S. Araki, T. C. Kobayashi, M. Nakashima, Y. Amako, M. Hedo, T. Nakama, and Y. Ōnuki, Characteristic Fermi surfaces and charge density wave in $SrAl_4$ and related compounds with the $BaAl_4$-type tetragonal structure, J. Alloys Compd. **654**, 290 (2016).

[19] A. Nakamura, Y. Hiranaka, M. Hedo, T. Nakama, Y. Miura, H. Tsutsumi, A. Mori, K. Ishida, K. Mitamura, Y. Hirose, K. Sugiyama, F. Honda, R. Settai, T. Takeuchi, M. Hagiwara, T. D. Matsuda, E. Yamamoto, Y. Haga, K. Matsubayashi, Y. Uwatoko, H. Harima, and Y. Ōnuki, Magnetic and Fermi surface properties of $EuGa_4$, J. Phys. Soc. Jpn. **82**, 104703 (2013).

[20] S. Araki, Y. Ikeda, T. C. Kobayashi, A. Nakamura, Y. Hiranaka, M. Hedo, T. Nakama, and Y. Ōnuki, Charge density wave transition in $EuAl_4$, J. Phys. Soc. Jpn. **83**, 015001 (2013).

[21] A. Nakamura, Y. Hiranaka, M. Hedo, T. Nakama, Y. Miura, H. Tsutsumi, A. Mori, K. Ishida, K. Mitamura, Y. Hirose, K. Sugiyama, F. Honda, T. Takeuchi, T. D. Matsuda, E. Yamamoto, Y. Haga, and Y. Ōnuki, Unique Fermi surface and emergence of charge density wave in $EuGa_4$ and $EuAl_4$, JPS Conf. Proc. **3**, 011012 (2014).

[22] A. Nakamura, T. Uejo, F. Honda, T. Takeuchi, H. Harima, E. Yamamoto, Y. Haga, K. Matsubayashi, Y. Uwatoko, M. Hedo, T. Nakama, and Y. Ōnuki, Transport and magnetic properties of $EuAl_4$ and $EuGa_4$, J. Phys. Soc. Jpn. **84**, 124711 (2015).

[23] S. Shimomura, H. Murao, S. Tsutsui, H. Nakao, A. Nakamura, M. Hedo, T. Nakama, and Y. Ōnuki, Lattice modulation and structural phase transition in the antiferromagnet $EuAl_4$, J. Phys. Soc. Jpn. **88**, 014602 (2019).

[24] M. Kobata, S. Fujimori, Y. Takeda, T. Okane, Y. Saitoh, K. Kobayashi, H. Yamagami, A. Nakamura, M. Hedo, T. Nakama, and Y. Ōnuki, Electronic structure of $EuAl_4$ studied by photoelectron spectroscopy, J. Phys. Soc. Jpn. **85**, 094703 (2016).

[25] E. Fawcett and W. A. Reed, Effects of compensation on the galvanomagnetic properties of nonmagnetic and ferromagnetic metals, Phys. Rev. **131**, 2463 (1963).

[26] N. Nagaosa, J. Sinova, S. Onoda, A. H. MacDonald, and N. P. Ong, Anomalous Hall effect, Rev. Mod. Phys. **82**, 1539 (2010).

[27] M. Lee, Y. Onose, Y. Tokura, and N. P. Ong, Hidden constant in the anomalous Hall effect of high-purity magnet MnSi, Phys. Rev. B **75**, 172403 (2007).

[28] Y. Tian, L. Ye, and X. Jin, Proper Scaling of the Anomalous Hall Effect, Phys. Rev. Lett. **103**, 087206 (2009).

[29] D. Hou, G. Su, Y. Tian, X. Jin, S. A. Yang, and Q. Niu, Multivariable Scaling for the Anomalous Hall Effect, Phys. Rev. Lett. **114**, 217203 (2015).

[30] J. J. Ying, Y. J. Yan, A. F. Wang, Z. J. Xiang, P. Cheng, G. J. Ye, and X. H. Chen, Metamagnetic transition in $Ca_{1-x}Sr_xCo_2As_2$ ($x = 0$ and 0.1) single crystals, Phys. Rev. B **85**, 214414 (2012).

[31] M. Kakihana, D. Aoki, A. Nakamura, F. Honda, M. Nakashima, Y. Amako, S. Nakamura, T. Sakakibara, M. Hedo, T. Nakama, and Y. Ōnuki, Giant Hall resistivity and magnetoresistance in cubic chiral antiferromagnet EuPtSi, J. Phys. Soc. Jpn. **87**, 023701 (2017).

[32] Y. Xu, L. Das, J. Z. Ma, C. J. Yi, Y. G. Shi, A. Tiwari, S. S. Tsirkin, T. Neupert, M. Medarde, M. Shi, J. Chang, and T. Shang, Topological transverse transport in the presence and absence of long-range magnetic order in $EuCd_2As_2$, arXiv:2008.05390.

[33] P. Puphal, V. Pomjakushin, N. Kanazawa, V. Ukleev, D. J. Gawryluk, J. Ma, M. Naamneh, N. C. Plumb, L. Keller, R. Cubitt, E. Pomjakushina, and J. S. White, Topological Magnetic Phase in the Candidate Weyl Semimetal CeAlGe, Phys. Rev. Lett. **124**, 017202 (2020).

[34] S. Mühlbauer, B. Binz, F. Jonietz, C. Pfleiderer, A. Rosch, A. Neubauer, R. Georgii, and P. Böni, Skyrmion lattice in a chiral magnet, Science **323**, 915 (2009).

[35] X. Z. Yu, N. Kanazawa, Y. Onose, K. Kimoto, W. Z. Zhang, S. Ishiwata, Y. Matsui, and Y. Tokura, Near room-temperature formation of a skyrmion crystal in thin-films of the helimagnet FeGe, Nat. Mater. **10**, 106 (2011).

[36] X. Z. Yu, Y. Onose, N. Kanazawa, J. H. Park, J. H. Han, Y. Matsui, N. Nagaosa, and Y. Tokura, Real-space observation of a two-dimensional skyrmion crystal, Nature (London) **465**, 901 (2010).

[37] S. Seki, X. Z. Yu, S. Ishiwata, and Y. Tokura, Observation of skyrmions in a multiferroic material, Science **336**, 198 (2012).

[38] I. Kézsmárki, S. Bordács, P. Milde, E. Neuber, L. M. Eng, J. S. White, H. M. Rønnow, C. D. Dewhurst, M. Mochizuki, K. Yanai, H. Nakamura, D. Ehlers, V. Tsurkan, and A. Loidl, Néel-type skyrmion lattice with confined orientation in the polar magnetic semiconductor GaV_4S_8, Nat. Mater. **14**, 1116 (2015).

[39] Y. Tokunaga, X. Z. Yu, J. S. White, H. M. Rønnow, D. Morikawa, Y. Taguchi, and Y. Tokura, A new class of chiral materials hosting magnetic skyrmions beyond room temperature, Nat. Commun. **6**, 7538 (2015).

[40] S. Seki, J.-H. Kim, D. S. Inosov, R. Georgii, B. Keimer, S. Ishiwata, and Y. Tokura, Formation and rotation of skyrmion crystal in the chiral-lattice insulator Cu_2OSeO_3, Phys. Rev. B **85**, 220406(R) (2012).

[41] M. Hirschberger, T. Nakajima, S. Gao, L. Peng, A. Kikkawa, T. Kurumaji, M. Kriener, Y. Yamasaki, H. Sagayama, H. Nakao, K. Ohishi, K. Kakurai, Y. Taguchi, X. Yu, T. Arima, and Y. Tokura, Skyrmion phase and competing magnetic orders on a breathing kagomé lattice, Nat. Commun. **10**, 5831 (2019).

[42] H. Li, B. Ding, J. Chen, Z. Li, Z. Hou, E. Liu, H. Zhang, X. Xi, G. Wu, and W. Wang, Large topological Hall effect in a geometrically frustrated kagome magnet Fe_3Sn_2, Appl. Phys. Lett. **114**, 192408 (2019).

[43] N. D. Khanh, T. Nakajima, X. Yu, S. Gao, K. Shibata, M. Hirschberger, Y. Yamasaki, H. Sagayama, H. Nakao, L. Peng, K. Nakajima, R. Takagi, T. Arima, Y. Tokura, and S. Seki, Nanometric square skyrmion lattice in a centrosymmetric tetragonal magnet, Nat. Nanotechnol. **15**, 444 (2020).

[44] X. Z. Yu, Y. Tokunaga, Y. Kaneko, W. Z. Zhang, K. Kimoto, Y. Matsui, Y. Taguchi, and Y. Tokura, Biskyrmion states and their current-driven motion in a layered manganite, Nat. Commun. **5**, 3198 (2014).

[45] C. D. Batista, S.-Z. Lin, S. Hayami, and Y. Kamiya, Frustration and chiral orderings in correlated electron systems, Rep. Prog. Phys. **79**, 084504 (2016).

[46] H. Niki, S. Nakamura, N. Higa, H. Kuroshima, T. Toji, M. Yogi, A. Nakamura, M. Hedo, T. Nakama, Y. Ōnuki, and H. Harima, Studies of ^{27}Al NMR in $EuAl_4$, J. Phys.: Conf. Ser. **592**, 012030 (2015).

[47] In the momentum-space scenario, the term “anomalous Hall effect” is often used in the literature to denote any contribution other than the ordinary Hall effect. Here, we use the term “topological Hall effect” to denote the contribution in addition to the ordinary and the *conventional* anomalous Hall effect, as determined from magnetization measurements. In other words, the topological Hall effect we discuss here is the topologically nontrivial part of the anomalous Hall effect.

[48] S. Nakatsuji, N. Kiyohara, and T. Higo, Large anomalous Hall effect in a non-collinear antiferromagnet at room temperature, Nature (London) **527**, 212 (2015).

[49] M. Ikhlas, T. Tomita, T. Koretsune, M.-T. Suzuki, D. Nishio-Hamane, R. Arita, Y. Otani, and S. Nakatsuji, Large anomalous Nernst effect at room temperature in a chiral antiferromagnet, Nat. Phys. **13**, 1085 (2017).

[50] T. Suzuki, R. Chisnell, A. Devarakonda, Y.-T. Liu, W. Feng, D. Xiao, J. W. Lynn, and J. G. Checkelsky, Large anomalous Hall effect in a half-Heusler antiferromagnet, Nat. Phys. **12**, 1119 (2016).

[51] C. Y. Guo, F. Wu, Z. Z. Wu, M. Smidman, C. Cao, A. Bostwick, C. Jozwiak, E. Rotenberg, Y. Liu, F. Steglich, and H. Q. Yuan, Evidence for Weyl fermions in a canonical heavy-fermion semimetal YbPtBi, Nat. Commun. **9**, 4622 (2018).

[52] A. K. Nayak, J. E. Fischer, Y. Sun, B. Yan, J. Karel, A. C. Komarek, C. Shekhar, N. Kumar, W. Schnelle, J. Kübler, C. Felser, and S. S. P. Parkin, Large anomalous Hall effect driven by a nonvanishing Berry curvature in the noncolinear antiferromagnet Mn_3Ge, Sci. Adv. **2**, e1501870 (2016).